

Vacuum Polarization Energy of a Proca Soliton

Damian A. Petersen^{a)}, Herbert Weigel^{a)}

^{a)}*Institute of Theoretical Physics, Physics Department,
Stellenbosch University, Matieland 7602, South Africa*

We study an extended Proca model with one scalar field and one massive vector field in one space and one time dimensions. We construct the soliton solution and subsequently compute the vacuum polarization energy (VPE) which is the leading quantum correction to the classical energy of the soliton. For this calculation we adopt the spectral methods approach which heavily relies on the analytic properties of the Jost function. This function is extracted from the interaction of the quantum fluctuations with a background potential generated by the soliton. Particularly we explore eventual non-analytical components that may be induced by mass gaps and the unconventional normalization for the longitudinal component of the vector field fluctuations. By numerical simulation we verify that these obstacles do actually not arise and that the real and imaginary momentum formulations of the VPE yield equal results. The Born approximation to the Jost function is crucial when implementing standard renormalization conditions. In this context we solve problems arising from the Born approximation being imaginary for real momenta associated with energies in the mass gap.

I. INTRODUCTION

We consider solitons as static finite energy solutions to non-linear field equations [1–3]. Examples for these solutions are Skyrmions [4, 5], monopoles in $(3 + 1)$ dimensions and vortices, strings and lumps in $(2 + 1)$ dimensions. There are numerous applications in various branches of physics: in cosmology [6], condensed matter physics [7, 8], as well as hadron and nuclear physics [9]. We point to those textbooks and review articles for more details and further references.

The field equations minimize the classical energy. Here we are, however, mostly interested in the vacuum polarization energy (VPE) which is the corresponding leading quantum correction. It has been corroborated that spectral methods, which utilize scattering data for the quantum fluctuations about the static potential generated by the soliton are a very efficient technique to compute the VPE [10]. This is especially the case for implementing standard renormalization conditions because the Born series of the scattering data is equivalent to the Feynman series of the one-loop effective action. Even more, the analytic properties of the Jost function, which is a particular solution to the scattering wave-equation, allow us to express the VPE as a single integral over imaginary momenta, and makes the method even more efficient [11]. For a particular model it is therefore compulsory to ensure that there is no obstacle for the underlying analytic continuation. Here we will discuss two situations for which such obstacles seem to exist.

For the scattering problem for two (or more) fields with masses $m_1 \leq m_2$, the Born approximation to the sum of the phase shifts contains a contribution proportional to

$$\frac{1}{\sqrt{k^2 - m_2^2 + m_1^2}} \int dx v_{>}(x),$$

where $v_{>}$ is the self-interaction potential of the heavier particle. Obviously this is ill-defined (or imaginary) for momenta $k \in [0, \sqrt{m_2^2 - m_1^2}]$ which correspond to energies in the mass gap. However, the Born approximation is a crucial element for implementing standard renormalization conditions. In Ref. [12] this problem was circumvented by analytical continuation $k = it$ so that the denominator becomes $\pm i\sqrt{t^2 + m_2^2 - m_1^2}$ and is only needed for $t \geq m_1$. Hence it is important to verify the validity of the analytic continuation when computing the VPE.

We face another possible obstacle in the Proca model for a vector meson field V_α with mass μ . For a free Proca field in $D = 1 + 1$ dimensions this field only has temporal (V_0) and longitudinal (V_1) components. The former is not dynamical (its time derivative does not appear in the Lagrangian) and its elimination yields an extended relation between the field velocity and the canonical momentum:

$$\Pi_1(t, x) = \dot{V}_1(t, x) + \frac{1}{\mu^2} \Pi_1''(t, x). \quad (1)$$

Here, and in what follows, dots and primes are time and space derivatives, respectively. The second term in Eq. (1) requires the field decomposition

$$V_1(t, x) = \int \frac{dk}{2\pi(2\omega)} \frac{\omega}{\mu} \left[a^\dagger(k) e^{-i(\omega t - kx)} + a(k) e^{i(\omega t - kx)} \right], \quad (2)$$

so that $a(k)$ and $a^\dagger(k)$ are respectively annihilation and creation operators for vector particles with energy $\omega = \sqrt{k^2 + \mu^2}$. While the energy factor in the integration measure is standard¹, its appearance in the ratio $\frac{\omega}{\mu}$ is unconventional and the corresponding square root discontinuity might hamper the analytic continuation in the momentum variable k .

After this introduction we will briefly review the spectral methods approach to the VPE in Chapter II. We will especially explain the effectiveness of the imaginary momentum formulation. In Chapter III we will consider a toy model for two scalar fields with different masses. We will present a solution to the above mentioned Born obstacle and, by numerical simulation, we will verify that the real and imaginary momentum formulations yield identical results. In Chapter IV we will introduce a Proca model in $D = 1 + 1$ space-time dimensions and construct its soliton solution. Thereafter, in Chapter V, we will investigate the scattering problem in that model with emphasis on the role of the non-standard normalization of the longitudinal mode. Chapter VI contains our numerical results for the VPE of the Proca soliton. We will briefly summarize and outline related future projects in Chapter VII.

The VPE can also be computed from scattering formulations of the Green's functions [13, 14]. Alternatively, the fluctuation determinant is directly computed (or estimated) within heat kernel methods [15] in conjunction with ζ -function renormalization [16], or by the world line formalism [17]. Other approaches relate the quantum fields with and without the soliton background by a displacement operator [18], conduct derivative expansions [19], or apply the Gel'fand-Yaglom method [20]; just to name a few other techniques. The implementation of standard renormalization conditions is not too obvious in most of these approaches. This is even more the case when these techniques are applied to models that contain quadratic divergences. Also, the unbiased reader should be able to easily assess the superior efficiency of the spectral methods when comparing the discussion in Sect. II with, for example, the heat kernel formalism detailed in the appendix of Ref. [21] or the lengthy and highly technical calculations in Ref. [18].

II. BRIEF REVIEW OF SPECTRAL METHODS

The VPE is the renormalized shift of the zero point energies for the quantum fluctuations about the soliton background. For a static background the bosonic VPE is formally given by

$$E_{\text{VPE}} = \frac{1}{2} \sum_k \left(\omega_k - \omega_k^{(0)} \right) + E_{\text{CT}}. \quad (3)$$

Here ω_k and $\omega_k^{(0)}$ are the energy eigenvalues of the fluctuations about the background of the soliton and the translationally invariant vacuum, respectively. Furthermore E_{CT} is the counterterm contribution that implements the renormalization. It is part of the model definition but needs to be adjusted at each order in the perturbation/loop expansion.

The formal sum in Eq. (3) can be expressed as a discrete sum over bound states plus a continuum integral over scattering states. The latter are labeled by their momentum k , with $\omega_k = \sqrt{k^2 + m^2}$. That integral is conveniently evaluated using the Friedel-Krein formula [22],

$$\Delta\rho = \frac{1}{\pi} \frac{d\delta(k)}{dk} \quad (4)$$

for the change in the density of states, $\Delta\rho$, generated by the soliton background. Here we imply the sum over channels. For the projects mentioned in the introduction it suffices to consider the case of one space dimension. When the potential is reflection invariant² this sum is over channels with spatially symmetric and anti-symmetric wave-functions and $\delta(k)$ is the sum of the respective phase shifts. When needed, we will refer to this sum as the total phase shift. We then evaluate the continuum part in Eq. (3) as an integral with the measure $\Delta\rho dk$

$$\begin{aligned} E_{\text{VPE}} &= \frac{1}{2} \sum_j^{\text{b.s.}} \omega_j + \int \frac{dk}{2\pi} \sqrt{k^2 + m^2} \frac{d\delta(k)}{dk} + E_{\text{CT}} \\ &= \frac{1}{2} \sum_j^{\text{b.s.}} \omega_j + \int_0^\infty \frac{dk}{2\pi} \sqrt{k^2 + m^2} \frac{d}{dk} [\delta(k) - \delta_B(k)] + E_{\text{FD}} + E_{\text{CT}} \end{aligned}$$

¹ It is usually compensated by the very same factor in the commutation relation $[a(k), a^\dagger(k')] = 2\pi(2\omega)\delta(k - k')$.

² A more general case has been considered in Ref. [23].

$$= \frac{1}{2} \sum_j^{\text{b.s.}} (\omega_j - m) + \int_0^\infty \frac{dk}{2\pi} \left[\sqrt{k^2 + m^2} - m \right] \frac{d}{dk} [\delta(k) - \delta_B(k)] + E_{\text{FD}} + E_{\text{CT}}. \quad (5)$$

The discrete sum now only involves the isolated bound state energies $|\omega_j| < m$. In the second line we have subtracted the leading terms of the Born series for the phase shift. The (smallest) number of these terms is determined such that the momentum integral is finite. The Born contributions to the VPE can alternatively be expressed as Feynman diagrams, E_{FD} , which we use to add back the preceding subtractions under the integral. These diagrams are regularized by standard means (*e.g.* dimensional regularization) and $E_{\text{FD}} + E_{\text{CT}}$ remains finite when the regulator is removed. For boson models in one space dimension the only required Feynman diagram is proportional to the spatial integral over the background potential. Thus we can implement the no-tadpole renormalization condition in the form $E_{\text{FD}} + E_{\text{CT}} = 0$. In the third line of Eq. (5) we have used Levinson's theorem that relates the phase shift at zero momentum to the number of bound states³.

A central element of potential scattering theory is the Jost solution $f_k(x)$. It solves the wave-equation subject to the asymptotic condition

$$\lim_{x \rightarrow \infty} f_k(x) e^{-ikx} = 1 \quad (6)$$

and is analytic in the upper half momentum plane, *i.e.* for $\text{Im}(k) \geq 0$ [25]. For spatially symmetric potentials the Jost function $F(k)$ is extracted from $f_k(0)$ and $f'_k(0)$. (Below we will give more details when discussing particular models.) Obviously the Jost function is also analytic for $\text{Im}(k) \geq 0$ and for real k its phase is the scattering phase shift

$$F(k) = |F(k)| e^{-i\delta(k)}.$$

While the modulus $|F(k)|$ is an even function of real k , the phase is odd. This can be easily understood from the asymptotic condition above: Since the wave-equation is real, that condition implies that $k \rightarrow -k$ corresponds to complex conjugation. For an arbitrary function $g = g(k^2)$ we thus have

$$\int_0^\infty \frac{dk}{2\pi} g(k^2) \frac{d}{dk} [\delta(k)]_B = \frac{i}{2} \int_{-\infty}^\infty \frac{dk}{2\pi} g(k^2) \frac{d}{dk} [\ln F(k)]_B,$$

where the subscript indicates the necessary subtractions from the Born series. We use the Jost function to compute Eq. (5) by completing the contour in the upper half k -plane. The Born subtraction ensures that there is no contribution from the semi-circle at $|k| \rightarrow \infty$. It remains to collect the residues and bypass the branch-cut along the imaginary axis induced by $g(k^2) = \sqrt{k^2 + m^2} - m$. Another well-established property of the Jost function is that it has single roots which are located on the imaginary axis at the wave-numbers of the bound state energies [25]: $\kappa_j = \sqrt{m^2 - \omega_j^2}$ which implies

$$\frac{d}{dk} \ln F(k) \approx \frac{1}{k - i\kappa_j} \quad \text{for} \quad k \approx i\kappa_j.$$

Hence the pole contributions cancel against the (explicit) bound state sum in Eq. (5). The branch cut is along the imaginary axis starting at $k = im$. We introduce $k = it$, recognize that the square root discontinuity is $2i\sqrt{t^2 - m^2}$ and finally obtain

$$E_{\text{VPE}} = \int_m^\infty \frac{dt}{2\pi} \frac{t}{\sqrt{t^2 - m^2}} [\ln F(it)]_B \quad (7)$$

for a boson theory in $D = 1 + 1$ dimensions within the no-tadpole renormalization scheme. In the renowned sine-Gordon and ϕ^4 -kink models the total Jost functions are known [11]

$$F_{\text{sG}}(it) = \frac{t - m}{t + m} \quad \text{and} \quad F_{\text{kink}}(it) = \frac{t - m}{t + m} \frac{2t - m}{2t + m}.$$

Direct integration yields the well-established results for the VPE: $-\frac{m}{\pi}$ and $\frac{m}{12\pi} (\sqrt{3}\pi - 18)$, respectively [1]. This calculation clearly illustrates the effectiveness of the imaginary axis formulation.

³ See Ref. [24] for the formulation of Levinson's theorem in one space dimension.

III. REAL AXIS CALCULATION

As we will see, the effectiveness of the imaginary axis formulation is even more pronounced for systems with coupled scattering channels and different mass parameters. We will always consider two such channels with the convention that the mass parameters are ordered $m_1 \leq m_2$. The other case is merely a matter of re-labeling.

The imaginary axis formulation has already been established some time ago [12]. Nevertheless and precisely because of that, it is necessary to verify that it agrees with the real axis approach, Eq. (3). The latter is hampered not only by the Born obstacle mentioned in the introduction but also by the proper identification of the phase shift, which in the direct numerical simulation is obtained in the interval $[-\pi, \pi]$. As will be discussed below, with the existence of threshold cusps that endeavor may be cumbersome. We will investigate these issues within a toy model defined by a spatially symmetric 2×2 potential matrix $V(x) = (v_{ij}(x))$. We combine the two fields ϕ_1 and ϕ_2 into a two-component array $\psi = (\phi_1, \phi_2)^t$ which obeys the wave-equation

$$\ddot{\psi}(x, t) - \psi''(x, t) = -M^2\psi(x, t) - V(x)\psi(x, t). \quad (8)$$

with the diagonal mass matrix $M^2 = \text{diag}(m_1^2, m_2^2)$. Since the potential is static we can factorize the time dependence as $\psi(x, t) = \psi_k(x)e^{-i\omega t}$ where $k = \sqrt{\omega^2 - m_1^2}$ is a unique label. Furthermore we define a matrix of Jost solutions where the entries of a particular column are the two fields ϕ_1 and ϕ_2 while the different columns refer to solutions to the wave-equation that asymptotically have outgoing plane waves for only one of the two fields. To be precise we write

$$F_k(x) = Z_k(x) \begin{pmatrix} e^{ikx} & 0 \\ 0 & e^{ik_2x} \end{pmatrix} \quad \text{with} \quad k_2 = k_2(k) \equiv k \sqrt{1 - \frac{m_2^2 - m_1^2}{[k + i0^+]^2}}. \quad (9)$$

The particular form of the dependent momentum k_2 ensures the pertinent behavior under $k \rightarrow -k$ (symmetric in the gap, but anti-symmetric outside) and that all additional singularities will reside in the lower half complex k -plane [12]. The coefficient matrix is subject to the second order differential equation

$$Z_k''(x) = -2Z_k'(x)D(k) + [M^2, Z_k(x)] + V(x)Z_k(x) \quad \text{with} \quad D(k) = i \begin{pmatrix} k & 0 \\ 0 & k_2 \end{pmatrix}. \quad (10)$$

The asymptotic condition, Eq. (6) translates into $\lim_{x \rightarrow \infty} Z_k(x) = \mathbf{1}$. The Born series is straightforwardly constructed by iterating $Z_k(x) = \mathbf{1} + Z_k^{(1)}(x) + Z_k^{(2)}(x) + \dots$, where the superscripts refer to the order in the background potential $V(x)$. That is, $V(x)$ is the source for $Z_k^{(1)}(x)$, $V(x)Z_k^{(1)}(x)$ is the source for $Z_k^{(2)}(x)$ and so on. All $Z_k^{(l)}(x)$ vanish at spatial infinity.

The scattering wave-functions are linear combinations of $F_k(x)$ and $F_k^*(x) = F_{-k}(x)$ and the relative weight is the scattering matrix. In the anti-symmetric (-) and symmetric (+) channels the wave-function and its derivative, respectively, vanish at the center of the potential. From that we get the scattering matrices. Since we are only interested in the total phase shift we consider $\det[S_{\pm}(k)] = \det[F_{\pm}(-k)F_{\pm}^{-1}(k)]$ with the Jost matrices

$$F_+(k) = \lim_{x \rightarrow 0} [Z'(k, x)D^{-1}(k) + Z(k, x)] \quad \text{and} \quad F_-(k) = \lim_{x \rightarrow 0} Z(k, x). \quad (11)$$

Finally, the total phase shift is given by

$$\delta(k) = -\text{Im}(\text{Lndet}[F_+(k)F_-(k)]). \quad (12)$$

One reason for the $i0^+$ prescription in Eq. (9) is to ensure that e^{ik_2x} decays exponentially for momenta in the mass gap regardless of the sign of k . For that reason we can use Eq. (12) also in that momentum regime when the second particle channel is closed.

The fact that the wave-function in the symmetric channel has a boundary condition on its derivative leads to a slight modification of Levinson's theorem in one space dimension [24]:

$$\delta(0) = \pi \left(n - \frac{1}{2} \right). \quad (13)$$

As $\delta(k)$ is the sum of the phase shifts in the symmetric and anti-symmetric channels, so is n the total number of bound states from these two channels.

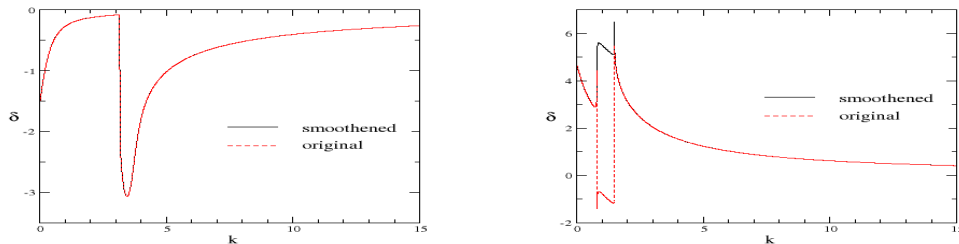


FIG. 1: Total phase shift in the toy model for repulsive (left) and attractive (right) potentials. The parameters for the repulsive case are $m_1 = 1.5$, $m_2 = 3.5$, $\bar{v}_{11} = 4.0$, $\bar{v}_{22} = 2.5$ and $\bar{v}_{12} = \bar{v}_{21} = 2.0$. In that case the two lines are on top of each other. The attractive potential is parameterized by $m_1 = 2.0$, $m_2 = 2.5$, $\bar{v}_{11} = -4.0$, $\bar{v}_{22} = -3.0$ and $\bar{v}_{12} = \bar{v}_{21} = -0.5$.

For later consideration the Born approximation is extracted from

$$\begin{aligned} \lim_{x \rightarrow 0} \text{tr} \ln \left(\left[Z^{(1)'}(k, x) D^{-1}(k) + \mathbf{1} + Z^{(1)}(k, x) \right] \left[\mathbf{1} + Z^{(1)}(k, x) \right] \right) \\ \approx \lim_{x \rightarrow 0} \text{tr} \left(Z^{(1)'}(k, x) D^{-1}(k) + 2Z^{(1)}(k, x) \right). \end{aligned}$$

Multiplying the first order expansion of equation (10) with $D^{-1}(k)$ from the right and integrating from zero to infinity yields⁴

$$\delta_B(k) = -\frac{1}{k} \int_0^\infty dx v_{11}(x) - \frac{1}{k_2} \int_0^\infty dx v_{22}(x). \quad (14)$$

Of course, this expression is only well-defined outside the mass gap where $k_2 \in \mathbb{R}$.

In numerical simulations equation (12) only produces results in the interval $[-\pi, \pi]$ which, in particular when there are bound states, does not produce a smooth function of k that vanishes as $k \rightarrow \infty$. To this end we apply a smoothening algorithm by evaluating equation (12) on a dense grid for discretized momenta and add multiples of 2π on identified intervals such that the difference of the phase between two neighboring momenta does not exceed 1.05π . This produces a smooth function to which we eventually add $\pm 2\pi$ to accommodate the large k limit. However, this procedure is delicate when the actual phase shift indeed has sharp cusps as it is the case at the top end of the mass gap or for Feshbach resonances [26] just below the mass gap. It may therefore still happen that this smoothening procedure fails to yield the correct phase shift within the gap. We can test for that by inverting Levinson's theorem, Eq. (13): We determine the bound state energies numerically by applying a shooting method to the differential equation for $\psi_{i\kappa}(x)$ such that the wave-function is continuous and vanishes exponentially as $x \rightarrow \infty$. This is possible only for discrete values of $|\omega_j| \leq m_1$. Once we have found these bound state energies, we also know n and thus the correct value $\delta(0)$. If it does not match the result from the smoothing method, we need to add (or subtract) appropriate integer multiples of $2\pi(m_1 - m_2)/2\pi = m_1 - m_2$ to the VPE. Eventually we will also probe the so computed VPE against the imaginary axis calculation. In Fig. 1 we display characteristic results for this smoothening procedure for the toy model potential $v_{ij}(x) = \bar{v}_{ij}e^{-x^2}$. For attractive potentials there are no bound states and the original and smoothened phases are identical. On the other hand, for (strongly) attractive potentials this need not be the case. For the example with the attractive potential used in Fig. 1 we find bound states at $\omega_1 = 1.256$ and $\omega_2 = 1.960$ in the symmetric and anti-symmetric channels, respectively. Hence we should have $\delta(0) = \frac{3}{2}\pi$, as is obeyed by the smoothened phase. Yet, the violent behavior of the original phase shift indeed indicates that there are numerical subtleties.

We next address the problem associated with the Born subtraction. Obviously we cannot use the exact Born approximation, Eq. (14) in Eq. (5). Rather, we consider

$$\tilde{E}_{\text{VPE}} = \frac{1}{2} \sum_k^{\text{b.s.}} (\omega_k - m_1) - \int_0^\infty \frac{dk}{2\pi} \frac{k}{\sqrt{k^2 + m_1^2}} [\delta(k) - \Delta(k)], \quad (15)$$

⁴ Note that $\text{tr}([M^2, Z^{(1)}(k, x)] D^{-1}(k)) = 0$.

with $\Delta_B(k) = -\frac{1}{k} \int_0^\infty dx [v_{11}(x) + v_{22}(x)]$. We will show that the difference to E_{VPE} can be calculated in two ways that yield identical results: (i) by a reparameterization of the momentum integral and (ii) the difference of two Feynman diagrams.

Since the Born approximation only concerns the diagonal elements of the potential matrix it suffices to consider a single channel problem with a spatially symmetric potential $v(x)$ in the channel with the heavier mass. With the definition $\langle V \rangle = -\int_0^\infty dx v(x)$ the corresponding VPE is

$$\begin{aligned} E_2 &= \frac{1}{2} \sum_j^{\text{b.s.}} (\omega_j - m_2) - \int_0^\infty \frac{dk}{2\pi} \frac{k}{\sqrt{k^2 + m_2^2}} \left[\delta(k) - \frac{\langle V \rangle}{k} \right] \\ &= \frac{1}{2} \sum_j^{\text{b.s.}} (\omega_j - m_2) - \int_{\sqrt{m_2^2 - m_1^2}}^\infty \frac{dq}{2\pi} \frac{q}{\sqrt{q^2 + m_1^2}} \left[\delta\left(\sqrt{q^2 - m_2^2 + m_1^2}\right) - \frac{\langle V \rangle}{\sqrt{q^2 - m_2^2 + m_1^2}} \right], \end{aligned}$$

with the new integration variable $q = \sqrt{k^2 - m_1^2 + m_2^2}$. According to equation (15) we would calculate

$$\tilde{E}_2 = \frac{1}{2} \sum_j^{\text{b.s.}} (\omega_j - m_1) - \int_0^\infty \frac{dq}{2\pi} \frac{q}{\sqrt{q^2 + m_1^2}} \left[F(q) - \frac{\langle V \rangle}{q} \right],$$

with

$$F(q) = \begin{cases} n_2 \pi = \delta(0) & \text{for } q^2 \leq m_2^2 - m_1^2 \\ \delta\left(\sqrt{q^2 - m_2^2 + m_1^2}\right) & \text{for } q^2 \geq m_2^2 - m_1^2, \end{cases}$$

where n_2 is the number of bound states in that channel and the smoothing produces the $q^2 \leq m_2^2 - m_1^2$ part. The contribution of that part is obtained from

$$\int_0^{\sqrt{m_2^2 - m_1^2}} \frac{dq}{2\pi} \frac{n_2 \pi q}{\sqrt{q^2 + m_1^2}} = \frac{n_2}{2} \sqrt{q^2 + m_1^2} \Big|_0^{\sqrt{m_2^2 - m_1^2}} = \frac{1}{2} \sum_j^{\text{b.s.}} (m_2 - m_1).$$

This allows us to write

$$\begin{aligned} \tilde{E}_2 &= \frac{1}{2} \sum_j^{\text{b.s.}} (\omega_j - m_2) + \int_0^{\sqrt{m_2^2 - m_1^2}} \frac{dq}{2\pi} \frac{\langle V \rangle}{\sqrt{q^2 + m_1^2}} \\ &\quad - \int_{\sqrt{m_2^2 - m_1^2}}^\infty \frac{dq}{2\pi} \frac{q}{\sqrt{q^2 + m_1^2}} \left[\delta\left(\sqrt{q^2 - m_2^2 + m_1^2}\right) - \frac{\langle V \rangle}{q} \right], \end{aligned}$$

resulting in

$$\begin{aligned} E_2 - \tilde{E}_2 &= - \int_0^{\sqrt{m_2^2 - m_1^2}} \frac{dq}{2\pi} \frac{\langle V \rangle}{\sqrt{q^2 + m_1^2}} + \int_{\sqrt{m_2^2 - m_1^2}}^\infty \frac{dq}{2\pi} \frac{q}{\sqrt{q^2 + m_1^2}} \left[\frac{\langle V \rangle}{\sqrt{q^2 - m_2^2 + m_1^2}} - \frac{\langle V \rangle}{q} \right] \\ &= \int_0^\infty \frac{dq}{2\pi} \left[\frac{\langle V \rangle}{\sqrt{q^2 + m_2^2}} - \frac{\langle V \rangle}{\sqrt{q^2 + m_1^2}} \right] = \frac{\langle V \rangle}{2\pi} \ln \frac{m_1}{m_2}. \end{aligned} \tag{16}$$

Next we look at the one-loop effective action arising from the fluctuations and single out the $\mathcal{O}(V)$ contribution:

$$\begin{aligned} \Delta\mathcal{A}^{(1)} &= \frac{i}{2} \text{Tr} \left[(\partial^2 + m_1^2 - i\epsilon)^{-1} v - (\partial^2 + m_2^2 - i\epsilon)^{-1} v \right] \\ &= \frac{i}{2} \int \frac{d^2k}{(2\pi)^2} \left[(-k^2 + m_1^2 - i\epsilon)^{-1} - (-k^2 + m_2^2 - i\epsilon)^{-1} \right] \tilde{v}(0), \end{aligned}$$

	\tilde{E}_{vac} Eq. (15)	$E_{\text{vac}} - \tilde{E}_{\text{vac}}$ Eq. (18)	E_{vac}	E_{vac} Eq. (19)
repulsive	-0.5102	0.4780	-0.0322	-0.0324
attractive	-0.0872	-0.0944	-0.1817	-0.1821

TABLE I: Comparison of real and imaginary axis calculation of the VPE for the Gaussian potential matrix $v_{ij} = \bar{v}_{ij}e^{-x^2}$. Model parameters are as in Fig. 1.

where \tilde{v} is the Fourier transform of $v(x)$ so that $\tilde{v}(0) = \int d^2x v(x) = -2\langle V \rangle T$, with T denoting an (infinitely large) time interval. The above integral is straightforwardly evaluated by Wick rotation yielding

$$\Delta\mathcal{A}^{(1)} = -\frac{\langle V \rangle T}{2\pi} \ln \frac{m_1}{m_2}. \quad (17)$$

The corresponding effective energy matches Eq. (16). Hence using Eq. (15) for the real axis calculation and correcting it with Eq. (16) properly implements the no-tadpole condition. Essentially we regulate the ultra-violet divergence from the heavier particle by a Feynman diagram with the lighter particle in the loop. We may consider this treatment as a variant of the Pauli-Villars regularization scheme. In the two channel problem we write the correction as

$$E_{\text{vac}} - \tilde{E}_{\text{vac}} = \frac{\langle V \rangle}{2\pi} \ln \frac{m_{<}}{m_{>}} \quad \text{with} \quad \langle V \rangle = -\int_0^\infty dx v_{>}(x). \quad (18)$$

Here the subscripts refer to the smaller (<) and larger (>) of the two masses and $v_{>}$ again is the self-interaction component of potential matrix for the heavier particle.

The goal is to compare the numerical results from the approach outlined above to the imaginary momentum procedure discussed in Chap. II. The latter has been generalized to the two-component system in Ref. [12]. We need to solve Eq. (10) with the replacements $k \rightarrow t = ik$ and $k_2 \rightarrow i\sqrt{t^2 + m_2^2 - m_1^2}$ to write the VPE as

$$E_{\text{vac}} \equiv \frac{1}{2\pi} \int_0^\infty d\tau \left[\nu(t) - \nu^{(1)}(t) \right]_{t=\sqrt{\tau^2 + m_1^2}}, \quad (19)$$

with

$$\nu(t) \equiv \ln \det [F_+(it) F_-(it)] \quad \text{and} \quad \nu^{(1)}(t) = \int_0^\infty dx \left[\frac{v_{11}(x)}{t} + \frac{v_{22}(x)}{\sqrt{t^2 + m_2^2 - m_1^2}} \right]. \quad (20)$$

Clearly there is no singularity in the Born approximation, $\nu^{(1)}$. We also note that the $F_\pm(it)$ are real-valued matrices. In Tab. I we compare the results for the two scenarios of Fig. 1. The agreement of the two approaches could not be clearer. We have performed numerous such comparisons [27] and never obtained mismatches in the leading three significant digits after rounding the fourth one.

The considerable lower cost of computing time makes the imaginary axis approach significantly more efficient. This is mainly caused by the smoothing procedure which requires a dense discretization for the real momenta. Also the fact that the real axis approach solves a differential equation for a complex matrix rather than a real one adds computing time. On top there is the advantage that the imaginary axis approach does not require to explicitly find the bound state energies. Nevertheless this toy model exercise impressively confirms the equivalence of the real and imaginary momentum computations of the VPE, even in the presence of potential branch cuts arising from energy thresholds. We will use that knowledge to explore the potential non-analyticity in a vector meson Proca model in Chap. V. But first we need to construct that soliton.

IV. PROCA SOLITON

We consider a Lagrangian in $D = 1 + 1$ space time dimensions with two real fields: a scalar (Φ) and a massive vector meson (V_α)

$$\mathcal{L} = \frac{1}{2} \partial_\alpha \Phi \partial^\alpha \Phi - \frac{1}{4} (\partial_\alpha V_\beta - \partial_\beta V_\alpha)^2 + \frac{\mu^2}{2} V_\alpha V^\alpha - \frac{1}{2} (\Phi^2 - 1)^2 - g (1 - \Phi^2) \epsilon^{\alpha\beta} V_\alpha \partial_\beta \Phi. \quad (21)$$

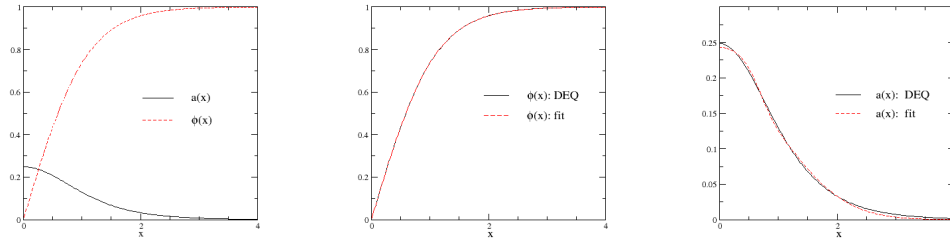


FIG. 2: Soliton profiles for $g = 1.0$ and $\mu = 1.5$ (left panel). Also shown are the fitted profiles for ϕ (middle panel) and a (right panel) in comparison with the solutions to Eq. (23); labeled 'DEQ'.

The scale is set by the scalar meson mass $m_\phi = 2$, the scalar self-interaction is that of the ϕ^4 kink model and the vector meson mass is μ . The coupling is constructed such that it is at least cubic in the fluctuations about the possible vacuum configurations ($\Phi_0 = \pm 1$ and $V_0^\alpha = 0$) and the ϵ tensor ensures that the field equations are consistent with $\partial^\alpha V_\alpha = 0$. The vector meson mass μ and the coupling constant g are the only tuneable model parameters. We have scaled variables, parameters and fields to dimensionless quantities. This produced an overall factor for \mathcal{L} which we do not explicitly write because it would only matter if we compared classical and quantum energies quantitatively. The model can be considered as the one-dimensional reduction of the Skyrme model with an ω meson [28]. This also motivates the soliton ansatz with a profile function only for the time component of the vector meson field, $V^\alpha = (a(x), 0)$ and $\Phi = \phi(x)$. The classical energy functional becomes

$$E_{\text{cl}} = \frac{1}{2} \int dx \left\{ \phi'^2 + (\phi^2 - 1)^2 - a'^2 - \mu^2 a^2 + 2g(1 - \phi^2)a\phi' \right\}. \quad (22)$$

The variational principle yields the static equations

$$a'' = \mu^2 a - g(1 - \phi^2)\phi' \quad \text{and} \quad \phi'' = 2\phi(\phi^2 - 1) - g(1 - \phi^2)a'. \quad (23)$$

For $g = 0$ they are solved by the ordinary kink, $\phi_K = \tanh(x)$ and $a \equiv 0$. Stable soliton solutions for $g \neq 0$ should also connect the two possible vacua $\phi_0 = \pm 1$ at positive and negative spatial infinity. This implies that ϕ is odd under the reflection around its center x_0 with $\phi(x_0) = 0$. We choose $x_0 = 0$ and find that $a(-x) = a(x)$. We solve Eqs. (23) with a shooting method on the positive half-line, $x \geq 0$ subject to the boundary conditions

$$\phi(0) = 0, \quad a'(0) = 0 \quad \text{and} \quad \lim_{x \rightarrow \infty} \phi(x) = 1, \quad \lim_{x \rightarrow \infty} a(x) = 0. \quad (24)$$

The profiles on the negative half-line, $x \leq 0$ can be constructed via the above discussed reflection properties. A typical solution is shown in the left panel of Fig. 2. For all cases considered, we have verified that

$$\int_0^\infty dx \{ \phi'^2 - a'^2 \} = \int_0^\infty dx \{ (\phi^2 - 1)^2 - \mu^2 a^2 \}$$

$$\text{and} \quad \int_0^\infty dx \{ a'^2 + \mu^2 a^2 - g(1 - \phi^2)a\phi' \} = 0 \quad (25)$$

are fulfilled. The first equation reflects Derrick's theorem [29] while the second is a consequence of stability under scaling the vector meson profile. Numerically these profiles are only known at prescribed values of the coordinate x . However, later in the scattering problem we will apply an adaptive step size algorithm which requires the profiles at other x values as well. Rather than implementing a (CPU time costly) interpolation, we choose to fit the profiles to analytic functions. A good choice is

$$\phi_{\text{fit}}(x) = a_0 \tanh(a_1 x) + a_2 \tanh(a_3 x) \quad \text{and} \quad a_{\text{fit}}(x) = b_0 e^{-b_1 x^2} + b_0 e^{-b_1 x^4}. \quad (26)$$

Even though there is some arbitrariness⁵ in $\phi_{\text{fit}}(x)$ we find fitting parameters that perfectly match the solution from the differential equation, as seen in the middle panel of Fig. 2. The fit to the vector profile shows some minor deviations

⁵ The fit algorithm consistently produced $a_0 + a_2 \approx 1$, see also Eq. (33) below.

μ	g	0.4	0.8	1.2	1.6	2.0
1.5	E_{cl}	1.356	1.422	1.532	1.679	1.858
	E_{fit}	1.356	1.423	1.533	1.680	1.860
2.5	E_{cl}	1.343	1.372	1.419	1.484	1.564
	E_{fit}	1.343	1.372	1.419	1.484	1.566

TABLE II: The classical energy, Eq. (22) for the solutions to the field equations, (23) and the fitted profiles, Eq. (26) as functions of the coupling constant g and two values of the vector meson mass m .

from the actual solution, in particular asymptotically as may be observed from the right panel in the same figure. In later applications we actually fit $a'(x)$ directly. In any event, we are typically able to construct fits that violate the identities in Eq. (25) by only about one in a thousand or less. This can also be seen from the data for the classical mass in Tab. II. From that table we see that the classical energy increases with the coupling constant. A bit more surprising is that it decreases as the vector meson mass gets larger. We may explain this by noting that for large μ the derivative term a'^2 may be omitted against $\mu^2 a^2$ and the field equation may be locally approximated by

$$a \approx \frac{g}{\mu^2} (1 - \phi^2) \phi'.$$

Then the vector meson profile is no longer dynamical and we may approximate the energy functional by

$$E_{\text{cl}} \approx \frac{1}{2} \int dx \left\{ \phi'^2 + (\phi^2 - 1)^2 + \frac{g^2}{\mu^2} (1 - \phi^2)^2 \phi'^2 \right\},$$

indicating that with growing μ we are left with the pure kink model which has classical energy $E_{\text{cl}}^{(\text{K})} = \frac{4}{3}$ for the units used here.

V. SCATTERING PROBLEM IN PROCA MODEL

We formulate the scattering problem by introducing small amplitude fluctuations about the above constructed soliton:

$$\Phi(x, t) = \phi(x) + e^{-i\omega t} \eta(x), \quad V_0(x, t) = a(x) + e^{-i\omega t} u_0(x) \quad \text{and} \quad V_1(x, t) = e^{-i\omega t} u_1(x). \quad (27)$$

The time dependences factorizes because the soliton is static and we omit to explicitly write the frequency (ω) dependence of the fluctuations η , u_0 and u_1 . With this parameterization the continuity equation $\partial^\alpha V_\alpha = 0$ reads $u_0 = -\frac{i}{\omega} u_1'$. This allows us to eliminate u_0 from the linearized field equations and obtain

$$u_1'' = (\mu^2 - \omega^2) u_1 - ig\omega (1 - \phi^2) \eta \quad (28)$$

$$\eta'' = (4 - \omega^2) \eta + 6(\phi^2 - 1) \eta + 2g\phi a' \eta + \frac{i}{\omega} \mu^2 (1 - \phi^2) u_1 + g^2 (1 - \phi^2)^2 \eta. \quad (29)$$

We immediately observe that the scattering problem is non-Hermitian. Rather, the coefficient functions of η in the differential equation for u_1 and its counterpart in the differential equation for η differ by factors $\frac{\omega}{\mu}$. When we introduce the scaled vector fluctuation \bar{u}_1 via⁶

$$u_1 = -i \frac{\omega}{\mu} \bar{u}_1, \quad (30)$$

the fluctuation equations indeed assume an Hermitian form,

$$\begin{aligned} \bar{u}_1'' &= (\mu^2 - \omega^2) \bar{u}_1 + g\mu (1 - \phi^2) \eta \\ \eta'' &= (4 - \omega^2) \eta + \left[6(\phi^2 - 1) + 2g\phi a' + g^2 (\phi^2 - 1)^2 \right] \eta + g\mu (1 - \phi^2) \bar{u}_1. \end{aligned} \quad (31)$$

⁶ See also Chap. 6 in Ref. [30].

	$\tilde{E}_{\text{b.s.}}$	$\tilde{E}_{\text{con.}}$	\tilde{E}_{vac}	$E_{\text{vac}} - \tilde{E}_{\text{vac}}$	E_{vac}	E_{vac}
$\mu = 1.5, g = 1.0$	-0.735	0.360	-0.375	-0.273	-0.648	-0.649
$\mu = 1.5, g = 1.2$	-0.735	0.353	-0.382	-0.272	-0.649	-0.649
$\mu = 1.5, g = 1.5$	-0.757	0.371	-0.387	-0.266	-0.653	-0.653
$\mu = 2.5, g = 1.0$	-1.146	0.459	-0.687	0	-0.687	-0.687
$\mu = 2.5, g = 1.2$	-1.164	0.453	-0.711	0	-0.711	-0.711
$\mu = 2.5, g = 1.5$	-1.172	0.440	-0.732	0	-0.732	-0.732

TABLE III: Comparison of the results from the real and imaginary momentum computations of the VPE in the Proca model for various model parameters. $\tilde{E}_{\text{b.s.}}$, $\tilde{E}_{\text{con.}}$ and \tilde{E}_{vac} respectively refer to the bound state, continuum pieces and their sum in Eq. (15) while $E_{\text{vac}} - \tilde{E}_{\text{vac}}$ is the Feynman diagram correction from Eq. (18). Finally the last column is the imaginary axis result from Eq. (19).

We observe the important feature that the rescaling in Eq. (30) compensates for the un-conventional normalization for longitudinal component in Eq. (2). That is, (without interactions) \bar{u}_1 is the wave-function of a single particle state that contributes $\frac{1}{2}\omega$ to the VPE. We find that the normalization issue and the construction of an Hermitian scattering problem are simply the two sides of the very same medal.

With this scaling the continuity equation is as simple as $\mu u_0 = -\bar{u}'_1$. Using the soliton equations (23) it is straightforward to verify that the above fluctuation equations with $\omega = 0$ are solved by $\eta = \phi'$ and $\bar{u}_1 = -\mu a$. The latter relation corresponds to $u_0 = a'$. Hence this zero mode is nothing but the (infinitesimal) translation of the soliton. Observing a zero mode in the bound state spectrum will further test the numerical simulations in Chap. VI.

For $\mu \geq 2$ we can now straightforwardly apply the formalism of Chap. III with $m_1 = 2$, $m_2 = \mu$ and the potential matrix

$$V = \begin{pmatrix} 6(\phi^2 - 1) + 2g\phi a' + g^2(\phi^2 - 1)^2 & g\mu(1 - \phi^2) \\ g\mu(1 - \phi^2) & 0 \end{pmatrix}. \quad (32)$$

In the other case, $\mu \leq 2$ we set

$$D(k) = i \begin{pmatrix} k_1 & 0 \\ 0 & k \end{pmatrix} \quad \text{with} \quad k_1 = k_1(k) = k \sqrt{1 - \frac{4 - \mu^2}{[k + i0^+]^2}}$$

in Eq. (10) and replace $m_1 \rightarrow \mu$ in Eq. (15).

VI. NUMERICAL RESULTS

In this section we present and discuss our numerical results for the VPE of the Proca soliton constructed above. We first mention that for all scenarios considered, we observe an energy eigenvalue in the symmetric channel at around $\omega_0 \approx 0.01 \dots 0.03$. This is the translational zero mode. It is not exactly at zero because of the discrepancy between the actual soliton profiles and the parameterizations in Eq. (26). This discrepancy provides an additional measure for the accuracy of the fit. Minor changes (for example using the fits from $g = 1.2$ for $g = 1.0$) in the fitted profiles fail to produce a low energy bound state at all.

We continue with the comparison of the real and imaginary momentum formalism as for the toy model in Sect. III. Six cases are listed in Tab. III. For $\mu = 2.5$ there is no contribution associated with the Feynman diagram correction in Eq. (18) because then the self-interaction potential for the heavier particle is zero. The table exhibits perfect agreement of the two approaches. Typically we observe differences at the fourth significant digit which, however, is out of the realm of the numerical precision. Obviously, it is possible to compute the VPE with both formalisms and, as expected from the analysis in the previous chapter, the normalization of the longitudinal component of the vector meson field does not hamper the analytic continuation.

For the above shown equivalence of the real and imaginary axis calculation, the fitting functions, Eq. (26) are good enough. However, for more quantitative discussions of the parameter dependence of the VPE a more ambitious parameterization might be needed. Also, as mentioned after Eq. (26) we directly fit a' because only that part of the vector profile enters the differential equation (31). We have considered a number of alternative parameterizations and found

$$\phi(x) \approx a_0 \tanh(a_1 x) + (1 - a_0) \tanh(a_2 x) \quad \text{and} \quad a'(x) \approx (b_0 + b_1 x^2 + b_2 x^4) x e^{-b_3 x^2} \quad (33)$$

g	0.4	0.8	1.2	1.6	2.0
$\mu = 1.0$	-0.655	-0.640	-0.624	-0.611	-0.609
$\mu = 1.5$	-0.662	-0.648	-0.657	-0.663	-0.682
$\mu = 2.0$	-0.670	-0.673	-0.688	-0.712	-0.757
$\mu = 2.5$	-0.670	-0.685	-0.718	-0.759	-0.826
$\mu = 3.0$	-0.673	-0.696	-0.737	-0.804	-0.890

TABLE IV: The vacuum polarization energy E_{VPE} for the Proca soliton as a function of the coupling constant g and for several values of the vector meson mass μ .

g	0.4	0.8	1.2	1.6	2.0
$\mu = 1.5$	–	–	1.499	1.429	1.330
$\mu = 2.0$	1.720	1.684*	1.629*	1.559*	1.478*
$\mu = 2.5$	1.724*	1.702*	1.665*	1.615*	1.556*

TABLE V: The bound state energy eigenvalues in the anti-symmetric channel as a function of the coupling constant and the Proca mass μ . Entries with a star indicate that there is second bound state (in addition to the zero mode) in the symmetric channel just below threshold at $\min(2, \mu)$.

to be most pertinent. We have assessed that from the predicted zero mode energy eigenvalue. The closer it is to zero, the more reliable is the considered parameterization. In most of the cases, however, there are only minor differences. For example, the case $\mu = 1.5$ and $g = 1.0$ yields $E_{\text{vac}} = -0.658$ and -0.649 for Eqs. (26) and (33), respectively. Generally we must allow a parameterization variance of one or two percent.

In Tab. IV we present the VPE as a function of the coupling constant g as obtained from the imaginary axis formulation, Eq. (19). After all, we have established its equivalence with the real axis formulation and it is much more efficient. Nevertheless we have verified this equivalence for selected cases.

When the scalar field is heavier than the Proca field, the VPE shows only little dependence on the coupling constant. The VPE is not even a monotonous function thereof. However, in the other regime, $\mu > 2$, the VPE considerably decreases as the coupling increases. It is a bit surprising that the Proca model VPE is close to the kink VPE (which in present units is $\frac{1}{6}(\sqrt{3} - \frac{18}{\pi}) \approx -0.666$ [1]) when the Proca field is the lighter one because lowering the threshold to $\mu < 2$ considerably alters the spectrum. In particular, the so-called *shape mode* bound state in the anti-symmetric channel, which in the kink model is at $\omega_1 = \sqrt{3} \approx 1.732$, may become unbound. Only when the coupling exceeds a certain value that bound state re-emerges. This is shown Tab. V. On the other hand, when $\mu \geq 2$ we observe a more moderate variation of this energy eigenvalue. Yet, the VPE changes considerably as a function of the coupling. Hence the change in the bound state spectrum is (partially) compensated by a similar one of the continuum spectrum. We view this as a manifestation of Levinson's theorem which tells us that altering the number of bound states has a significant impact on the phase shift.

The argument at the end of Chap. IV, that the kink model would be assumed for large μ , however, is not necessarily valid for time dependent fluctuations because there is always a frequency ω such that $\mu^2 - \omega^2$ is small and we may not generalize the local approximation to scattering wave-functions.

VII. CONCLUSION

The main objective of this project has been the investigation of the role of a potential non-analytic field normalization when computing the vacuum polarization energy (VPE) for a soliton containing a massive vector meson described by a Proca field. Fortunately it quickly became clear that this problem is closely related to the construction of an Hermitian scattering problem for the quantum fluctuations about the soliton. After that construction, the VPE calculation turned into that of two coupled scalar fields.

In verifying this conclusion by numerical simulation we have, as an important byproduct, established the equivalence of the real and imaginary momentum formalisms for computing the VPE when there is a mass gap. In this context the main accomplishment was to avoid the Born approximation because it is imaginary for fluctuation energies that are within the mass gap. We have used a particular helper function, motivated by the Pauli-Villars regularization scheme, and showed analytically as well as numerically that the resulting deviation from the no-tadpole condition is compensated by a finite Feynman diagram.

Numerically we have then constructed the soliton in a $D = 1 + 1$ model in which a Proca field interacts with a scalar one, solved the wave-equations for the small amplitude fluctuations about the soliton, and extracted the Jost function, both for real and purely imaginary momenta. This function is central to the spectral methods approach to compute the VPE. These methods are particularly efficient when the fluctuation momenta are continued to the imaginary axis.

While the classical energy increases with the coupling constant, the VPE either only varies mildly when the Proca field is the lighter of the two fields or decreases considerably with the coupling strength when the Proca field is the heavier one. A qualitative comparison of classical and quantum contributions to the energy would only be possible if the overall factor of the Lagrangian that acts as a loop-counter and emerges by scaling fields and coordinates to dimensionless quantities, was known.

Here we have considered the simplest model producing a massive vector meson soliton. Eventually we should consider higher dimensions and/or allow multiple scalar fields. The ultimate goal is the computation of the VPE of the 't Hooft-Polyakov monopole [31, 32]. Though numerically subtle, the heavy Proca mass limit is interesting because with the derivative coupling in Eq. (21) it potentially induces a non-trivial coefficient function for the kinetic term of the scalar field. A scenario for which a number of solitons have recently been constructed, *cf.* Ref. [33] which also quotes many articles that discuss models with such solitons. It seems infeasible to directly compute the VPE in such models because the wave-equations are not of the form, Eq. (8) as relative factors between the time and space derivatives may emerge.

Acknowledgments

D. A. P. acknowledges support by a bursary from the National Research Foundation of South Africa (NRF) and H. W. is supported in part by the NRF under grant 150672.

-
- [1] R. Rajaraman, *Solitons and Instantons* (North Holland, Amsterdam, 1982).
 - [2] N. S. Manton and P. Sutcliffe, *Topological Solitons*, Cambridge Monographs on Mathematical Physics (Cambridge University Press, 2004).
 - [3] T. Vachaspati, *Kinks and Domain Walls : An Introduction to Classical and Quantum Solitons* (Oxford University Press, 2010).
 - [4] T. H. R. Skyrme, Proc. Roy. Soc. Lond. **A260**, 127 (1961).
 - [5] I. Zahed and G. E. Brown, Phys. Rept. **142**, 1 (1986).
 - [6] A. Vilenkin and E. P. S. Shellard, *Cosmic Strings and Other Topological Defects* (Cambridge University Press, 2000).
 - [7] U. Schollwöck, *et al.*, *Quantum Magnetism*, vol. 645, Lecture Notes Phys. (Springer-Verlag, Berlin, 2004).
 - [8] N. Nagaosa and Y. Tokura, Nature Nanotech **8**, 1 (2013).
 - [9] H. Weigel, *Chiral Soliton Models for Baryons*, vol. 743, Lecture Notes Phys. (Springer-Verlag, Berlin, 2008).
 - [10] N. Graham, M. Quandt, and H. Weigel, *Spectral Methods in Quantum Field Theory*, vol. 777, Lecture Notes Phys. (Springer-Verlag, Berlin, 2009).
 - [11] N. Graham and H. Weigel, Int. J. Mod. Phys. A **37**, 2241004 (2022).
 - [12] H. Weigel, M. Quandt, and N. Graham, Phys. Rev. **D97**, 036017 (2018).
 - [13] J. Baacke, Z. Phys. **C47**, 263 (1990).
 - [14] N. Graham, R. L. Jaffe, V. Khemani, M. Quandt, M. Scandurra, and H. Weigel, Nucl. Phys. **B645**, 49 (2002).
 - [15] M. Bordag, J. Phys. **A28**, 755 (1995).
 - [16] E. Elizalde, *Ten Physical Applications of Spectral Zeta Functions*, vol. 855, Lecture Notes Phys. (Springer-Verlag, Berlin, 1995).
 - [17] H. Gies, K. Langfeld, and L. Moyaerts, JHEP **06**, 018 (2003).
 - [18] J. Evslin, JHEP **11**, 161 (2019).
 - [19] I. J. R. Aitchison, C. M. Fraser, Phys. Rev. **D31**, 2605 (1985).
 - [20] I. M. Gelfand and A. M. Yaglom, J. Math. Phys. **1**, 48 (1960).
 - [21] A. Alonso Izquierdo, W. Garcia Fuertes, M. A. Gonzalez Leon, J. Mateos Guilarte, Nucl. Phys. B **635**, 525 (2002).
 - [22] J. S. Faulkner, J. Phys. **C10**, 4661 (1977).
 - [23] H. Weigel, Phys. Lett. **B766**, 65 (2017).
 - [24] G. Barton, J. Phys. A **18**, 479 (1985).
 - [25] R. G. Newton, *Scattering Theory of Waves and Particles* (Springer, New York, 1982).
 - [26] H. Feshbach, Annals Phys. **5**, 357 (1958).
 - [27] D. A. Petersen, Master's thesis, Stellenbosch University (2024), unpublished.
 - [28] G. S. Adkins and C. R. Nappi, Phys. Lett. B **137**, 251 (1984).
 - [29] G. H. Derrick, J. Math. Phys. **5**, 1252 (1964).

- [30] B. Schwesinger, H. Weigel, G. Holzwarth, and A. Hayashi, Phys. Rept. **173**, 173 (1989).
- [31] G. 't Hooft, Nucl. Phys. B **79**, 276 (1974).
- [32] A. M. Polyakov, JETP Lett. **20**, 194 (1974).
- [33] E. da Hora, L. Pereira, C. dos Santos, and F. C. Simas (2024), 2409.09767.